ORIGINAL PAPER

Mechanomics analysis of hESCs under combined mechanical shear, stretch, and compression

Fan Zhang[1,2] · Jiawen Wang[1,2] · Dongyuan Lü[1,2] · Lu Zheng[1,2] · Bing Shangguan[1] · Yuxin Gao[1] · Yi Wu[1,2] · Mian Long[1,2]

Abstract
Human embryonic stem cells (hESCs) can differentiate to three germ layers within biochemical and biomechanical niches. The complicated mechanical environments in vivo could have diverse effects on the fate decision and biological functions of hESCs. To globally screen mechanosensitive molecules, three typical types of mechanical stimuli, *i.e.,* tensile stretch, shear flow, and mechanical compression, were applied in respective parameter sets of loading pattern, amplitude, frequency, and/ or duration, and then, iTRAQ proteomics test was used for identifying and quantifying differentially expressed proteins in hESCs. Bioinformatics analysis identified 37, 41, and 23 proteins under stretch pattern, frequency, and duration, 13, 18, and 41 proteins under shear pattern, amplitude, and duration, and 4, 0, and 183 proteins under compression amplitude, frequency, and duration, respectively, where distinct parameters yielded the differentially weighted preferences under each stimulus. Ten mechanosensitive proteins were commonly shared between two of three mechanical stimuli, together with numerous proteins identified under single stimulus. More importantly, functional GSEA and WGCNA analyses elaborated the variations of the screened proteins with loading parameters. Common functions in protein synthesis and modification were identified among three stimuli, and specific functions were observed in skin development under stretch alone. In conclusion, mechanomics analysis is indispensable to map actual mechanosensitive proteins under physiologically mimicking mechanical environment, and sheds light on understanding the core hub proteins in mechanobiology.

Abbreviations

ACY1	Aminoacylase-1
ANOVA	Analysis of variance
ANXA4	Annexin A4
BASP1	Brain abundant membrane attached signal protein 1
BP	Biological process
CC	Cellular component
CFL2	Cofilin 2
ES	Enrichment score
ESCs	Embryonic stem cells
EXOSC5	Exosome component 5
FC	Fold change
FDR	False discovery rate
GART	Phosphoribosylglycinamide formyltransferase
GO	Gene ontology
GSEA	Gene set enrichment analysis
hESCs	Human embryonic stem cells
HIST1H1B	Histone cluster 1 H1 family member b
HSP70	Heat shock protein family A
ITGB1	Integrin beta1
iTRAQ	Isobaric tags for relative and absolute quantitation

Fan Zhang and Jiawen Wang these authors contributed equally to this work.

✉ Mian Long
  mlong@imech.ac.cn

[1] Center for Biomechanics and Bioengineering, Key Laboratory of Microgravity (National Microgravity Laboratory) and Beijing Key Laboratory of Engineered Construction and Mechanobiology, Institute of Mechanics, Chinese Academy of Sciences, Beijing 100190, China

[2] School of Engineering Science, University of Chinese Academy of Sciences, Beijing 100049, China

LAMB1/C1   Lamin B1/C1
MAPK   Mitogen-activated kinase-like protein
mESCs   Mouse embryonic stem cells
MDC1   Mediator of DNA damage checkpoint 1
MF   Molecular function
MFI   Mean fluorescence intensity
MTHFD1   Methylenetetrahydrofolate dehydrogenase 1
NES   Normalized enrichment score
PCA   Principal component analysis
PHD   Plant homeodomain
PSMs   Protein spectrum matches
Q-Q plot   Quantile-sample quantile plot
RhoA   Ras homolog family member A
RPL35A   Ribosomal protein L35a
RT   Room temperature
STON2   Stonin 2
TFI   Total fluorescence intensity
UHRF1   Ubiquitin like with PHD and ring finger domains 1
WGCNA   Weighted gene co-expression network analysis
YAP   Yes associated protein 1

1 Introduction

Embryonic stem cells (ESCs) are obtained from inner cell mass of a 5-day blastocyst and are capable of self-renewal in vitro (Dado et al. 2012). ESCs can also differentiate into almost any cell types except umbilical cord and trophoblasts (Leeb et al. 2011). Human embryonic stem cell (hESC) line, first produced in 1998, is widely used as a model for studying the developmental processes of embryos and primitive gut formation and also serve as the basis of regenerative medicine (Thomson et al. 1998). These specialized stem cells are surrounded by matrices, cells, and tissues in vivo (so-called the niche), in which the biomechanical properties of the niche can affect their phenotypes (Conway and Schaffer 2012). Evidently, these mechanical environments play an important role in morphogenesis and organogenesis by regulating stem cell proliferation and differentiation (Heisenberg and Bellaiche 2013; Patwari and Lee 2008).

Embryo development starts from the fertilized egg and continues to differentiate into the specialized structures through persistent cell division and tissue remodeling, during which mechanical forces are always present. Oocyte is maturated along with enhanced osmotic pressure and activated intracellular calcium signals when moving from ovary to uterus (Horner and Wolfner 2008). Sperm acrosome exerts compression on oocyte to penetrate its physical barrier and then to accomplish the fertilization, followed by the consequent cell division and differentiation into distinct germ layers (Sanders et al. 1996; Shin et al. 2007). When

the primitive gut has formed, myosin in sectional cells is repositioned on the outer surface and then contracts the cells to generate the tension and to drive the ectocyst (Patwari and Lee 2008), resulting in the spreading of the enveloping cell layer (EVL) over the yolk cell (Behrndt et al. 2012). Fluid flow is required for blood vessel remodeling in embryonic angiogenesis. Prior to the appearance of the flow, mesoderm cells are first formed into a "blood island," and after the heart tube gains the functions, the flow appears and rapidly reconstitutes the blood vessels into arterial and venous branches (Patwari and Lee 2008). Mechanical stretch is also a key regulator in tissue morphogenesis. In implantation, the tension is induced by continuous cyclic extension of blastocyst when it escapes from the zona pellucida (Cole 1967) and then determines the polarity of embryo (Motosugi et al. 2005). These cues imply that mechanical stimuli are indispensable in ESCs' stemness maintenance and organogenesis. More importantly, different types of physiological mechanical stimuli (e.g., shear, stretch, or compression) are usually coupled with distinct patterns (e.g., steady, pulsatile, or oscillatory loading) and various parameters (e.g., amplitude, frequency, or duration), which forms one-to-more or more-to-one pattern between mechanical stimuli and biological responses (Wang et al. 2014).

ESCs have higher pluripotency and potentiate broader differentiation directions than adult stem cells. For instance, mechanical compression induces chondrogenic differentiation of mouse ESCs (mESCs) in 3-D PDMS scaffolds, accompanied by up-regulation of RhoA and YAP genes (McKee et al. 2017). mESCs placed on collagen type IV without LIF (leukemia inhibitory factor) and exposed to long-durations shear flow (4 days at 5 dyne/cm^2) present nearly twofold higher expression of mesodermal marker Brachyury than static control (Wolfe et al. 2012). A similar observation is that mESCs exposed to 10 dyne/cm^2 laminar flow for 24 h result in up-regulated expressions of mesodermal and cardiomyocyte markers of vascular endothelial growth factor 2 (VEGFR-2) and myocyte enhancer factor 2c (Mef2c) (Illi et al. 2005). Notably, these observations indicate the diversity of mechanical cues on regulating the stemness and differentiation of ESCs.

To date, global understanding how stem cells response to mechanical forces is still lacked (Ingber 2006). Cell mechanosensation and relevant mechanotransductive pathways attract much attention, which are related to numerous mechanosensitive genes, transcripts, and proteins. Moreover, transcriptomics/proteomics are widely used in mechanobiology to screen mechanosensitive molecules globally. For example, gene and protein profiles of bone tissues (Li et al. 2011), vascular endothelial cells (Chu and Peters 2008; Qi et al. 2011) and mesenchymal stem cells under shear stress (Kurpinski et al. 2009), engineered tendon formation under dynamic stretch (Jiang et al. 2011), osteoblasts cultured on

dissimilar hydroxyapatite biomaterials (Xu et al. 2008), as well as *Drosophila* (Herranz et al. 2012) and lymphoblastoid cells (Mangala et al. 2011) under simulated microgravity environment are extensively investigated, and novel mechanosensitive and signaling molecules are then revealed (Wang et al. 2014). While these studies are usually performed under a single mechanical stimulus, it is noticed that there are multiple types of mechanical stimuli in the microenvironment in which the cells reside in, with varied loading parameters under each type. When these mechanical factors act at the same time, the effects of each factor may be enhanced, counteracted, or even cancelled out with each other. Thus, it is critical to assess the interplay between various mechanical stimuli and cellular responses systematically. However, systematical screening of mechanosensitive molecules on multiple mechanical stimuli that mimics in vivo mechanical microenvironment is still lacked, especially for ESCs and in early organogenesis. Meanwhile, it is required to elaborate in-depth functions and mechanisms of those mechanosensitive molecules under systematically-varied mechanical stimuli.

Upon the concept of mechanomics newly proposed to define the multiple mechanical stimuli applied on single type of cells and elucidate the global molecular responses that the cells encounter (Wang et al. 2014), we hypothesized that there may exist fundamental mechanisms that are common in cell mechanobiology under combined mechanical stimuli. Here the mechanomics analysis was first carried out on human ESCs (hESCs) by determining proteome-level changes in response to various sets of in vitro mechanical combinations specifically for hESCs. Also compared were the differences in differential protein expressions under tensile stretch, shear flow, and mechanical compression with varied loading pattern, amplitude, frequency, and duration. The potential biological functions were also discussed from these analyses.

2 Materials and methods

2.1 Cell culture

hESC line H1 were from WiCell Research Institute (Madison, WI, https://www.wicell.org). hESCs were used to seed on six-well plate (Thermo Fisher, MA, USA) pre-coated with Matrigel (Corning, NY, USA) in mTeSR™ 1 medium (Stem Cell Technologies, Vancouver, BC, Canada). Cells were incubated at 37 °C in a humidified 5% (v/v) CO_2 atmosphere. The medium was exchanged once a day, and the cells were digested with dispase (Stem Cell Technologies) for 8 min at 37 °C for passage. Then the cells were scraped down with pipette tips in mTeSR™ 1 medium, resuspended

gently, and dispensed into a flow chamber plate or a new six-well plate before mechanical loading.

2.2 Application of mechanical stimuli

The cells after digestion were re-seeded onto an in-house built flow chamber plate or a commercialized six-well flexible silicone rubber BioFlex™ plate (BF-3001U-Case, Flexcell International Corporation, NC, USA) pre-coated with Matrigel. The seeded cells were incubated for 48 h prior to exposure to shear or stretch. For cells compression, the digested cells were collected by centrifuging at 800 rpm/min × 3 min and then embedded into 300 µL 3% (w/v) fluidic low melting-gel agarose (Solarbio, Beijing, China) in 37 °C. After being gently resuspended, all the liquid was aspirated onto the Bioflex™ plate (BF-3000C, Flexcell International Corporation) and the piston on the platen was screwed. Five milliliter medium was added into each well before mechanical compression. Then shear stress, mechanical strain, or contractile forces were applied, respectively, using an in-house built parallel-plate flow chamber, a commercial FX-4000™ tension unit or a FX-5000™ compression unit (FlexCell International Corporation) at given mechanical types and patterns, where the loading parameters are summarized in Fig. 1. Cultured cells were kept at 37 °C and humidified 5% (v/v) CO_2 atmosphere when being sheared, stretched, or compressed and then harvested or fixed immediately after mechanical loading at given duration indicated. For shear or stretch, the cells were digested with 0.25% Trypsin and lysed with lysis buffer (8 M urea) supplemented with 1 × protease inhibitor cocktail (Roche Applied Science, Basel, Switzerland). For compression, the agarose plugs were washed in 1 × PBS twice and immersed in liquid nitrogen immediately. Then the agarose plugs were carefully grinded into powders in mortar with liquid nitrogen and the lysis buffer was added at last. The collected sample was centrifuged at 12,000 rpm/min for 10 min, and the resulted supernatant was kept as protein solution. Two to three repeats for the cells exposed to the same stimulus were conducted, and all the proteins collected under this stimulus were pooled together for iTRAQ test.

2.3 Preparation for frozen sectioned samples after compression

For sample cryosectioning at the endpoint of a typical compression of 20 kPa at 1 Hz for 1 h, the agarose plugs with embedded H1 cells were washed in 1 × PBS twice, initially fixed in 4% paraformaldehyde (PFA) (Solarbio) at room temperature (RT) for 30 min, further embedded in OCT compound (Sakura Fineteck, Tokyo, Japan) and snap-frozen in liquid nitrogen, followed by trimming and sectioning the plugs into 10-µm-thick slices at −20 °C using a CM1950
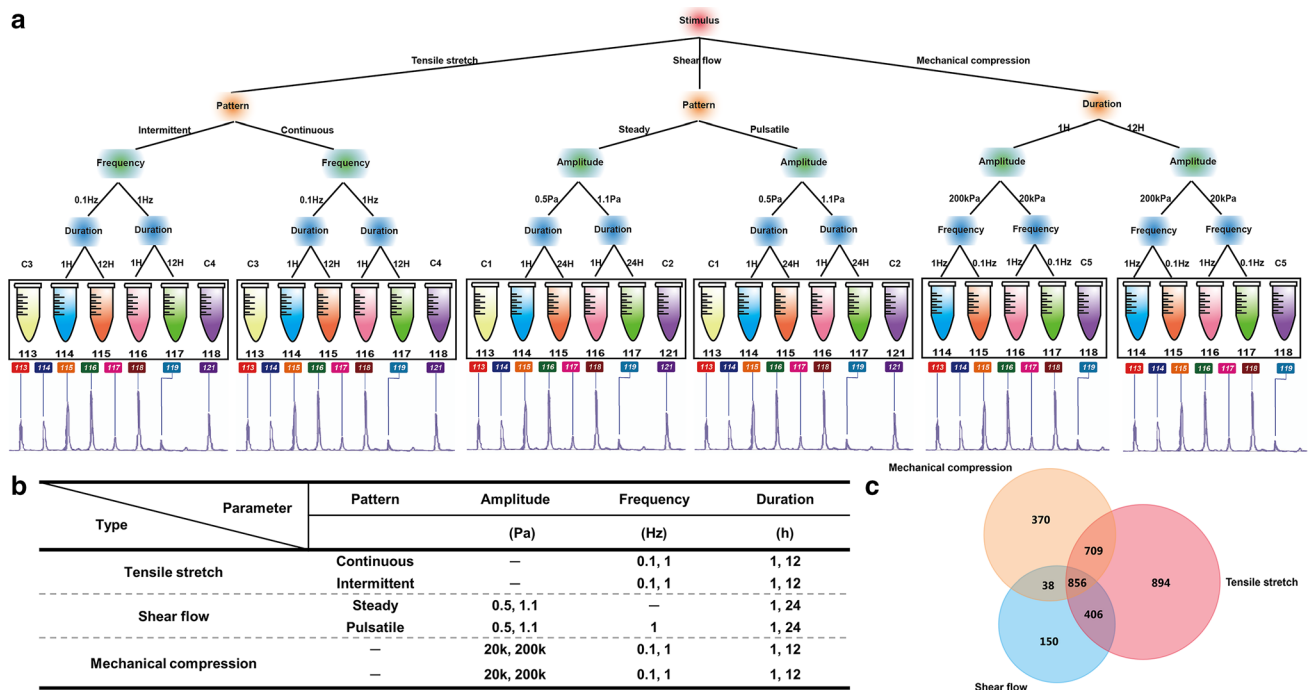
Fig. 1 Flowchart of mechanomics profiling for hESCs under tensile stretch, shear flow, or mechanical compression. **a** hESCs were exposed to tensile stretch, shear flow, or mechanical compression via in-house built parallel-plate flow chamber or commercial stretch and compression devices (Flexcell International, USA). Eight cases were adopted on each mechanical stimulus with varied loading patterns (steady or pulsatile, intermittent or continuous) and parameter sets (amplitude, frequency, and duration). Collected samples in each case were used for iTRAQ analysis in duplet with four mechanical groups and the corresponding control groups in each repeat. **b** Summaries of mechanical stimuli with varied loading patterns and parameter sets. **c** Intersection summaries of all proteins obtained from iTRAQ analysis under distinct mechanical stimuli. The colors denote the specific stimuli shown in **a**

cryoslicer (Leica Microsystems, Wetzlar, Germany) for subsequent immunofluorescence staining.

2.4 Immunofluorescent staining

H1 cells were seeded on the flow chamber plate for 2 days and then exposed to a steady flow of 1.1 Pa for 24 h. For stretch, H1 cells were seeded on the flexible silicone for two days and then exposed to an intermittent stretch at 0.1 Hz for 12 h. The sheared or stretched cells and those from static controls were then washed twice in $1 \times$ PBS and fixed with pre-chilled methanol (Concord, Tianjin, China) at $-20\ °C$ for 10 min. The RNASelect green fluorescent cell stain (Thermo Fisher) was diluted to a labeling solution in a concentration of 500 nM in PBS. The labeling solution was added into the above fixed cells, incubated for 20 min at RT in the dark, and then washed out twice in $1 \times$ PBS for 5 min. Hoechst 33342 (Thermo Fisher) staining reagent was diluted at 1:500 in $1 \times$ PBS and then applied on the labeled cells for 15 min at RT in the dark. After washed the cells twice in $1 \times$ PBS for 5 min, the confocal images were acquired with $40 \times$ or $63 \times$ oil objective on LSM 710 laser confocal microscope (Zeiss, Oberkochen, Germany). The slices under

compression were stained using the same protocol as the one under shear or stretch.

2.5 LC–MS/MS and data analysis

Cells after mechanical exposure were harvested and lysed for protein collection in each case (Fig. 1a and Table S1). Protein quality was confirmed using SDS-PAGE test (Fig. S1), confirming the integrality of protein collection. Protein concentration was determined using Bradford test, and all the samples were labeled with iTRAQ reagents upon the defined protocols (Fig. 1a) at given total amount of proteins (Table S2). For iTRAQ labeling, proteins collected from each sample were reduced with DTT (final concentration, 10 mM) at $56\ °C$ for 1 h, and alkylated with iodoacetamide (final concentration, 55 mM) in darkness at RT for 1 h. All samples were precipitated with quadruple volume of pre-chilled acetone at $-20\ °C$ and resolved with 300 μL TEAB buffer (0.5 M tetraethylammonium bicarbonate containing 0.1% (w/v) sodium dodecyl sulfate). After determining protein concentration, these protein solutions (totally 100 μg or 50 μg each) were subjected to tryptic hydrolysis at a ratio of enzyme to protein of 1:30 at $37\ °C$ for 24 h. After freeze drying, the tryptic peptides were resolved with 30 μL TEAB

buffer prior to be labeled with six-channel iTRAQ reagents (Applied Biosystems, Thermo Fisher) and evaporated to dryness in a vacuum concentrator 5301 (Eppendorf, Hamburg, Germany). The peptides were fractionated by strong cation exchange (SCX) chromatography (Phenomenex Luna SCX, 250×4.60 mm, 100 Å) on an Agilent 1000 HPLC system (Agilent, CA, USA). All peptide samples were separated on an online Dionex ultimate 3000 nano LC system (Thermo Fisher) and analyzed on a Q-Exactive hybrid quadrupole–orbitrap mass spectrometer (MS) (Thermo Fisher). Tandem mass spectra were screened using Proteome Discover (PD) 1.3 (Thermo Fisher) and then searched with Mascot (version 2.3.0, Matrix Science). Peak list files were searched against the NCBI_human for shear flow, the uniprot_2014_human (Wed Jan 22.2014 number of sequences 20,274) for tensile stretch, or the uniprot_20160315_human (Tue Mar 15 2016, Number of sequences: 20,199) for mechanical compression. Data were validated and quantified in PD using a threshold of identification of at least one unique peptide and at least 99% probability at the protein (peptide) level. iTRAQ ratio for each protein under various stimuli was defined as geometric mean of the ratio compared to technical duplicate of control samples. Relative protein abundance was quantified using the median of iTRAQ ratio for a given protein normalized to that of total measurable proteins. Statistical analysis of differential relative protein abundance was performed using three-way ANOVA test. $p < 0.015$ and fold change (FC) > 1.1 or < 0.9 were defined as significantly different proteins expressed under shear or stretch and $p < 0.015$ and FC > 1.5 or < 0.5 under compression, which will be discussed in the Results section.

2.6 Bioinformatics analysis

Unsupervised hierarchical clustering was conducted upon complete distance method. Distances between proteins and samples were computed using Spearman correlation coefficient of protein expression matrix under each stimulus. Clustering results and expression changes were rendered as heatmaps within the restrictions imposed by the dendrogram using heatmap.2 function of R packages gplots (version 3.0.1). Interaction network construct was performed using STRING database (https://string-db.org) and visualized with Cytoscape (version 3.3.0) (Shannon et al. 2003). CluePediaplugin (Bindea et al. 2009) of Cytoscape was used for proteome subcellular localization analysis. The top 20 proteins ranked by their degrees in the network were defined as pivot proteins and used to plot the network separately with the Cytohubba (Chin et al. 2014) of Cytoscape. The distributions of different proteins on chromosomes were elucidated with Circos (version 0.66) (Krzywinski et al. 2009). Gene Set Enrichment Analysis (GSEA) was performed on every parameter of all conditions against the Gene Ontology (GO)

gene sets, and FDR $< 25\%$ was set to define the enriched GO terms (Mootha et al. 2003; Subramanian et al. 2005). Weighted correlation network analysis was also performed among three mechanical stimuli via WGCNA (Langfelder and Horvath 2008; Vella et al. 2017), in which two modules that mostly correlate with the parameters of mechanical compression were selected to perform functional enrichment in GO term sets with clusterProfiler (Yu et al. 2012) and ggplot2 (Wickham 2016).

2.7 Statistical analysis

No repeated three-way ANOVA test with two levels was used to estimate the statistical significance of each loading factor in protein expression. For comparisons of nucleus or nucleolus features between any two groups, the unpaired two-tailed Student's t test was performed upon passing the normality test, or Mann–Whitney rank sum tests were used if not. P values of less than 0.05 were considered statistically significant.

3 Results

3.1 Collecting all the proteins under distinct mechanical stimuli

To obtain the global picture of hESCs mechanosensation, H1 cells were exposed to three types of mechanical stimuli, that is, tensile stretch, shear flow, and mechanical compression, with varied loading pattern, amplitude, frequency, and/or duration, respectively (Fig. 1a). Three loading parameters were set in each stimulus and 3 (types) $\times$ 3 (parameters) design of experimental (DOE) were applied, as summarized in Fig. 1b and Table S1. Here these mechanical parameters were mainly defined upon in vivo mechanical microenvironment or in vitro biomechanical studies for tensile stretch (Jiang et al. 2011; Rogers et al. 2012; Ward Jr et al. 2007), shear flow (Adamo et al. 2009; Braet et al. 2004; Malone et al. 2007; Qi et al. 2011; Sorescu et al. 2003; Stolberg and McCloskey 2009), or mechanical compression (Bonassar et al. 2001; Huang et al. 2005; Hur et al. 2011; Quinn et al. 1998). Cells after mechanical exposure were harvested, and collected proteins were labeled with iTRAQ reagents and detected using LC–MS/MS system. Analyzing the collected MS data presented the mechanosensitive proteins in the current settings. Specifically, 3302 and 3276 proteins were identified from intermittent and continuous stretch with 2865 commonly-shared proteins, 2016 and 2069 proteins from steady and pulsatile flow with 1450 shared, and 2551 and 2258 proteins form 1-h and 24-h compression with 1974 shared. In each type of stimulus, 76.7%, 55.0%, and 69.6% shared proteins were found in total proteins between

two patterns or durations of stretch, flow, and compression, respectively, implying that flow pattern may have significant impacts on mechanosensation of hESCs. Spanning over distinct types of stimuli, 1262, 894, and 1565 proteins were commonly shared between stretch and shear, shear and compression, or stretch and compression, respectively, and 856 among all the three stimuli (Fig. 1c). These results indicated that mechanical stimuli resulted in a large amount of commonly shared proteins, and those proteins not shared may be attributed to distinct mechanical stimuli or experimental batches.

To confirm iTRAQ test's reliability, linear regression analyses of protein spectrum matches (PSMs), unique peptides, and coverage were conducted for each protein identified from two independent iTRAQ tests. The slope of fitted line is 0.82–0.98 with correlation coefficient $R^2 = 0.851$–0.988 under each stimulus (Fig. S2a–i), suggesting the high repeatability and accuracy of protein identification from technical duplicates. Fold change (FC) of protein expression between mechanical loading group and no-loading control was normally distributed in all the eight cases under same stimulus, as exhibited by the distribution curves or theoretical quantile-sample quantile (Q–Q) plots (Fig. S3a–f), except one case of pulsatile flow at 0.5 Pa for 1 h (Fig. S3e), which was thus excluded from further analyses.

3.2 Screening differential proteins under distinct mechanical stimuli

To map those mechanically differential proteins, clustering analysis was done from the above twenty-three cases collectively. Cluster dendrogram (Fig. 2a) showed that three major clusters exist where each cluster is primarily composed of those proteins from single type of mechanical stimuli, suggesting that the loading type is dominant in the mechanosensitive responses of hESCs. Specifically, the priority of mechanical parameter clustering ranked in duration > pattern > frequency under stretch, duration > amplitude > pattern under shear, and duration > amplitude > frequency under compression. Distinct loading parameters played different roles in mechanosensitive protein expressions in single stimulus and highly prioritized parameters yielded similar clustering over multiple stimuli. Moreover, principal component analysis (PCA) using first three components indicated that most cases were clarified into separate clusters under each specific stimulus (separated *colored* circles), as the dendrogram did. Only one case of steady flow of 0.5 Pa for 1 h was close to those tensile stretch cases (Fig. 2b). Collectively, these results confirmed that the loading type is the most prioritized parameter.

A three-way ANOVA test was further used to calculate the *p*-value of all the proteins, which was integrated with FC value to define the mechanically differential proteins.

Considering the varied FC standard errors (SEs) from one to another stimulus, different thresholds of the combined two values were set under distinct stimuli, as specified in Fig. 2c. Here 37, 41, and 23 proteins were obtained for pattern, frequency, and duration under stretch, 13, 18, and 41 proteins for pattern, amplitude, and duration under shear, and 4, 0, and 183 proteins for amplitude, frequency, and duration for compression, respectively. As summarized for entire set of differential proteins in Table S4, those well-known mechanosensitive proteins of ITGB1, CFL2, and LAMB1/C1 were also displayed (Truong et al. 2015), partially confirming the availability of screening protocol. In addition, these mechanosensitive proteins were uniformly distributed in chromosomes (short black lines in the innermost circles in Fig. S4a–c), indicating that they have no preferences on specific chromatins. Considering the spatial structure of chromatin could alter the expressions of specific genes due to their location in the nucleus (Lemaitre and Bickmore 2015), mechanical loading may affect their expressions through changing chromatin arrangement directly.

3.3 Analyzing the biological functions of mechanically differential proteins

Subcellular localization of these mechanically differential proteins was classified by GO analysis and displayed as the axis from extracellular {1} through cell membrane {2}, cytosol {3}, nuclear membrane {4} to nucleus {5} and transcription factor {6} (Fig. 3). The majority of differential proteins yielded at least two localizations, which is able to be classified into three major categories. First is those from extracellular to cytosol, in total 99 proteins including {1, 3}, {2, 3}, and {1, 2, 3}, second from cytosol to nucleus in total 53 proteins of {2, 3, 5} and {3, 5}, and third directly from extracellular to nucleus in total 110 proteins of {1, 3, 5} and {1, 2, 3, 5} (Table S3). Together with those observations that shear flow and tensile stretch promotes transportation from extra- to intra-cellular regions and from cytosol to nucleus (Chahine et al. 2012; Ji et al. 2003; Lam and Dean 2008; Nithiananthan et al. 2016), such spatial distributions implied that frequent mass transfer and information exchange exist in mechanically loaded rather than no-loaded cells. While 77% mechanically differential proteins are transmembrane, protein translocation was more likely associated with cell membrane but not nuclear membrane, presumably due to the distinct functions of these two membranes. In fact, synthetic metabolism usually happens on the former whereas the latter is associated with nuclear translocation of those structural proteins through conformational changes induced by mechanical forces (Elosegui-Artola 2017).

Network interaction analysis was also conducted by importing the differential proteins into STRING database and screening the first 20 pivot proteins upon their degree
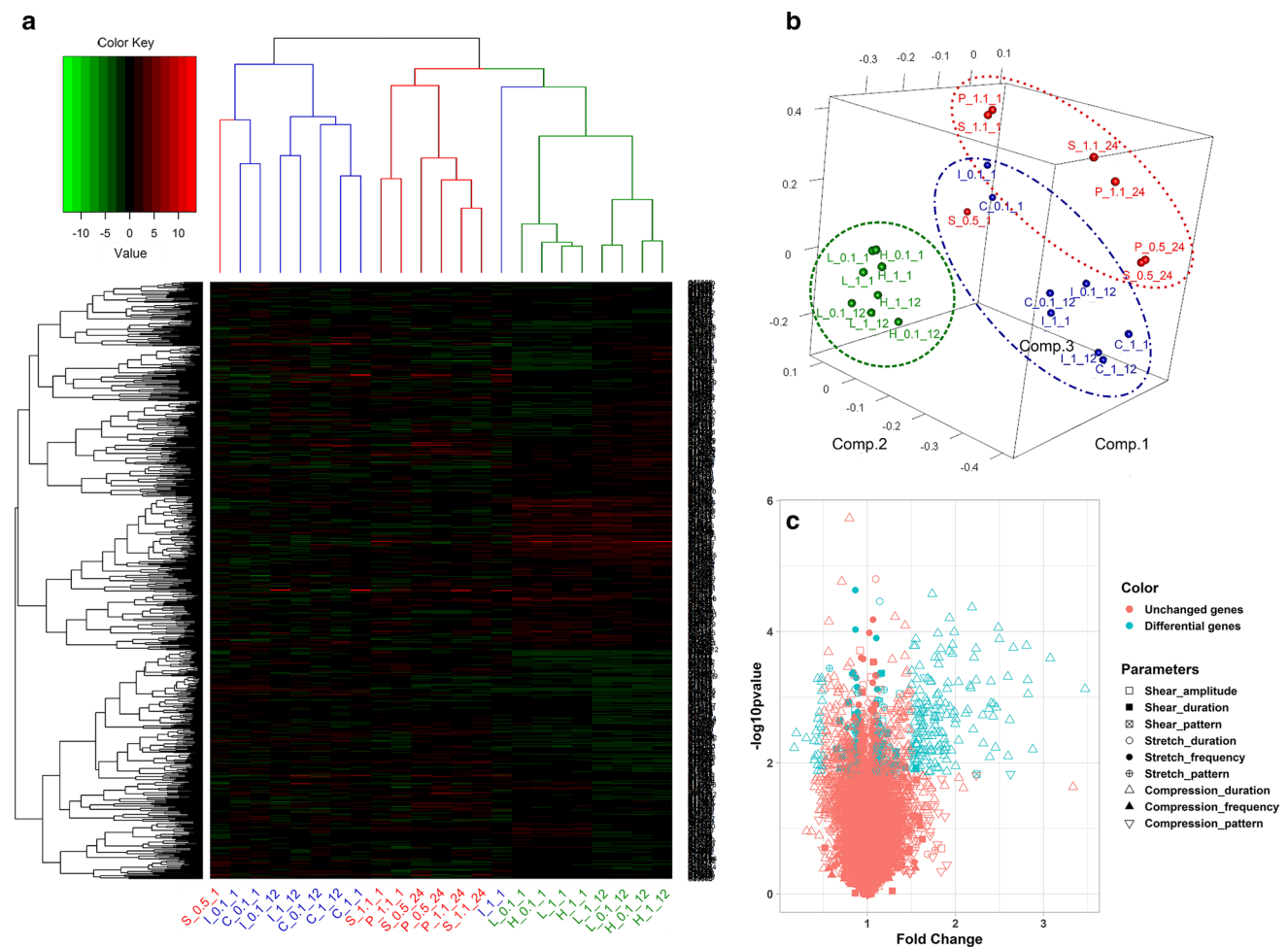
Fig. 2 Clustering analysis and differential protein screening under distinct mechanical stimuli. **a** Clustering of protein expressions in various cases of tensile stretch (blue), shear flow (red), and mechanical compression (green). Here x- or y-axis denoted the mechanical loading to each protein or the identity of the protein, and the dendrogram among columns or rows defined the correlation in mechanical stimuli or proteins. Branch length termed the distance of correlation coefficients between mechanical stimulus (Y-axis) and protein (X-axis) and the longer the branch is the farther the distance yields. **b** Principal component analysis (PCA) in all the cases of three mechanical stimuli represents in *red*, *blue* and *green* respectively. X-, Y- and Z-axes denote the first three principal components. **c** Volcano plot for differential protein screening upon their fold change (FC) and p-value. A threshold is given differentially under distinct stimuli, yielding FC > 1.1 or < 0.9 and p < 0.015 under shear flow and tensile stretch or FC > 1.5 or FC < 0.5 and p < 0.015 under mechanical compression. Red and blue colors denote undifferential and differential proteins, respectively

ranking under each stimulus (Fig. 4). Specifically, the proteins so obtained included DHX8, MRPS11, ATG7, UBE2G1, and EXOSC5 under stretch (**a**), RPL17, EEF1G, RPS15, RPS23, RPL14, and GART under shear (**b**), and CAD, CDK1, HSPD1, EEF2, and GART under compression (**c**). Only a few proteins were co-presented under two of three stimuli, *that is*, EXCSC5 between stretch and shear and GART between shear and compression. In addition, all the differentially expressed proteins were further compared to screen those commonly shared by any two or three mechanical stimuli. This turned out to be ten proteins, as shown in Table 1. For their subcellular localization, ACY1, MTHFD1, GART, and RPL35A lied in {1, 3}, EXOSC5, MDC1, STON2, UHRF1, and HIST1H1B in

{3, 5}, and BASP1 in {1, 2, 3, 5}. All of them yielded at least two localizations related to transmembrane trafficking, supporting that these conservative responses of hESCs to distinct stimuli are associated with mass transfer and signaling transduction. Moreover, the synergistic effects of these commonly shared proteins were also presented among distinct stimuli, when a synergistic or antagonistic action of a protein was defined as its consistent or opposite role under a specific parameter between two mechanical stimuli. For example, EXOSC5 expression was enhanced by long-duration loading under shear stress and tensile stretch, while GART was transiently enhanced in short duration, followed by a decay for long duration (Table 1). These observations indicated that common responding
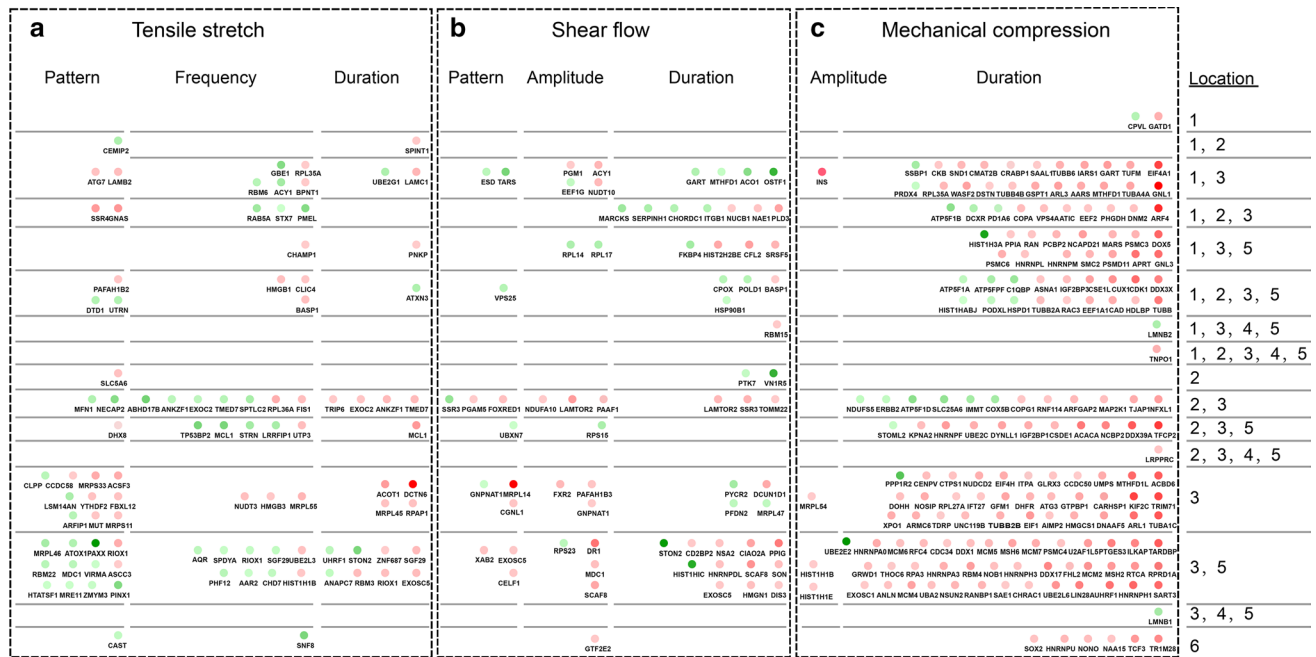
Fig. 3 Subcellular distributions of differential proteins under tensile stretch **a**, shear flow **b**, or mechanical compression **c**. Differential proteins obtained from various mechanical parameters are classified on each stimulus upon the orders of (1) extracellular, (2) plasma membrane, (3) intra cellular, (4) nuclear membrane, (5) nucleus and (6) transcription factor and then aligned together across distinct stimuli **a**–**c**. Each point denotes one type of up-regulated (red) or down-regulated (green) protein and the darkness of the point defines the fold change

mechanisms may exist in hESCs' responses to loading duration.

3.4 Comparing the mechanotransductive features of related biological functions

In contrast to the screening protocol upon FC and *p*-value that inevitably brings up the issue of threshold sensitivity, the GSEA method was further applied to conduct the enrichment analysis of the genes encoding mechanosensitive proteins under distinct parameters. All gene expressions were enriched upon pre-defined sets of biological process (BP), cellular component (CC), and molecular function (MF) and the resulted enrichment score (ES) was normalized to calculate the normalized enrichment score (NES) and FDR. Setting a threshold of FDR < 25% produced the enriched terms in each case (Fig. 5). Here the absolute value of *x*-axis denoted NES, and the positive or negative symbols represented the direction of enrichment towards the respective numerator or denominator defined in the caption. Figure 5a presents the terms enriched in CC and BP under all three stimuli, suggesting that the corresponding proteins are mechanosensitive. As exemplified in CC, the term "ribosome" was enriched in low-frequency (0.1 Hz) stretch, in high-amplitude (200 kPa) or high-frequency (1 Hz) compression, and in high-amplitude (1.1 Pa) or steady (0 Hz) shear. These outcomes implied that protein synthesis tends to be enriched along two opposite directions in loading frequency between stretch and compression, but be consistent in loading frequency between stretch and shear (low frequency) or in loading amplitude between shear and compression (high amplitude) (seen in *ribosome* term in Fig. 5a). Other terms associated with protein synthesis and transportation in CC and BP, such as "cytosolic ribosome" and "translational initiation," also presented similar enriching directions except that they were no longer enriched under steady shear. In contrast, an additional term in CC, "endoplasmic reticulum lumen," was related to protein modification and enriched along two opposite directions in loading frequency between stretch and compression or in loading duration between shear and compression. These analyses indicated that protein synthesis-related responses in hESCs are consistently enriched along high amplitude under all the types of stimuli but present the varied preferences in loading frequency and duration under distinct types of stimuli.

In addition, those terms commonly shared by any two of three stimuli in CC (Fig. 5b), BP (Fig. 5c), and MF (Fig. 5d) were also tested. Seventeen terms were enriched in CC. Besides the terms listed above, three typical subterms in CC, "large ribosomal subunit", "cytosolic large ribosomal subunit," and "cytosolic small ribosomal subunit," were found in opposite enrichment in loading
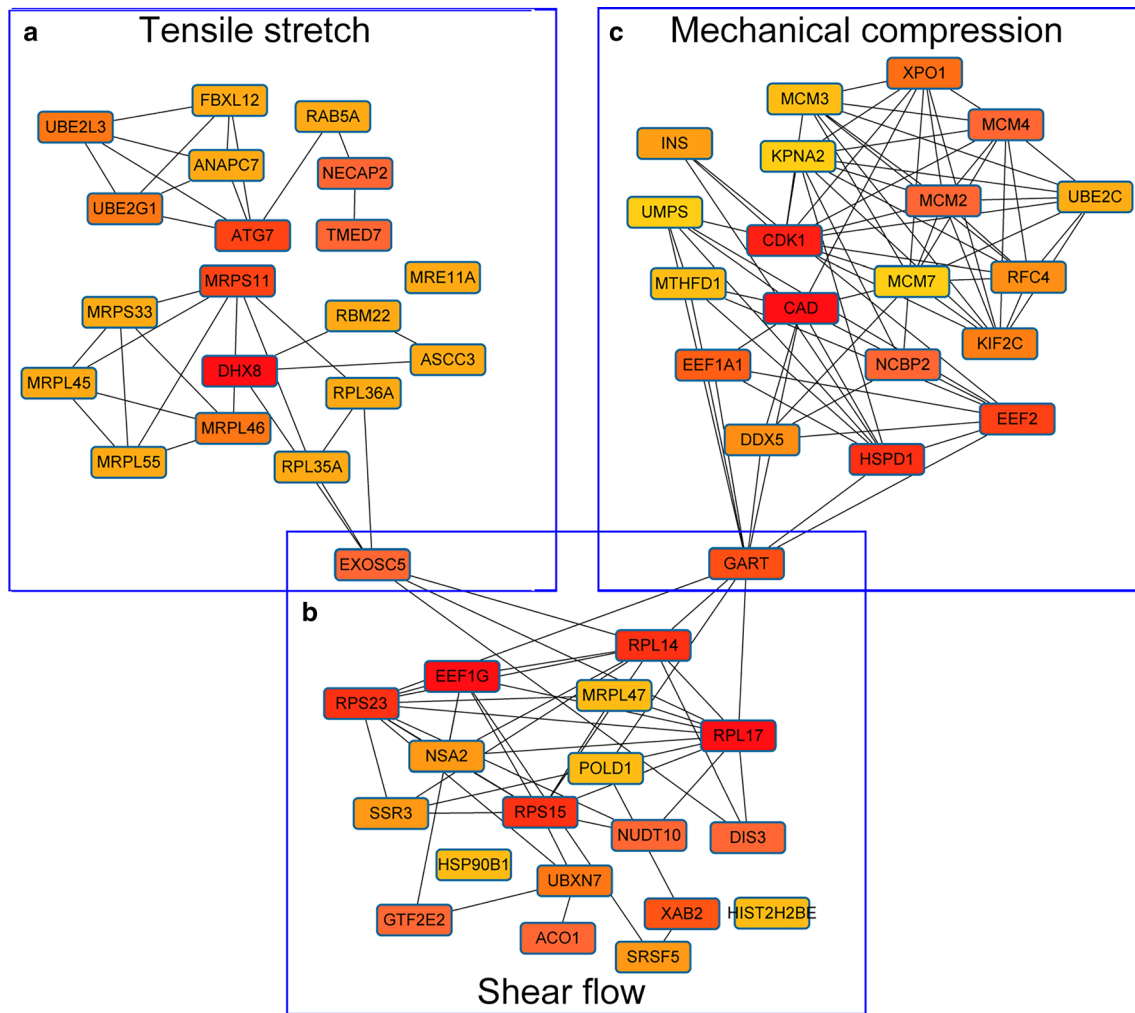
Fig. 4 Interaction network analysis of differential proteins under tensile stretch **a**, shear flow **b**, or mechanical compression **c**. Interaction network was constructed from differential proteins observed from STRING database under each stimulus. The first 20 pivot proteins were then screened upon their degree ranking using Cytoscape-cyto-hubba plug-in, where the colors from yellow to *red* denote the degree and pivot from low to high level. Note that GART and EXOSC5 are the hub proteins between mechanical compression and shear flow and between tensile stretch and shear flow, respectively

frequency between stretch and compression but in consistent enrichment in loading amplitude between shear and compression. By contrast, a sub-term "small ribosomal subunit" was enriched in high loading amplitude between shear and compression but not responsible in loading frequency between stretch and compression. These analyses indicated that these key pathways or terms in protein synthesis and transportation could be segregated into sub-pathways or sub-terms to further identify the multiple mechanotransductive mechanisms involved. Compared with CC, relatively fewer terms were enriched in BP and MF. The enriched terms in BP were similar to those among three stimuli. Typically, one term "protein localization to organelle" was enriched in high compression frequency and high shear amplitude and another "ribosome biogenesis" enriched in high compression frequency and long

shear duration. In MF, one typical term "structure specific to DNA binding" was enriched in high amplitude between shear and compression and another "chaperone binding" enriched in 1-h shear and 12-h compression, both different from those in CC and BP. Evidently, functional enrichment between any two of three stimuli presented more abundant, in-depth terms.

For enrichment in CC, BP, and MF under single mechanical stimuli, plenty of terms were enriched in various parameter settings under tensile stretch (total 26 terms), shear flow (total 58 terms), or mechanical compression (total 391 terms) (Table S4). As exemplified in Fig. S5, typical 5–7 terms under each parameter were enriched along two opposite directions upon the definition in S5a, presenting the functional diversity in CC (S5b), BP (S5c), and MF (S5d).

Table 1 Summaries of differential mechanosensitive proteins commonly shared by any two of three distinct mechanical stimuli

Types	Protein	Description	Regular pattern
Shear flow versus tensile stretch	EXOSC5	Exosome component 5	Synergistic effect (long-duration, high expression)[a]
	MDC1	Mediator of DNA damage checkpoint 1	N/C (high expression under continuous stretch and low-amplitude shear)[b]
	ACY1	Aminoacylase-1	N/C (high expression under 1-Hz stretch and low-amplitude shear)
	STON2	Stonin 2	Synergistic effect (short duration, high expression)
	BASP1	Brain abundant membrane attached signal protein 1	N/C (high expression under 0.1-Hz stretch and long-duration shear)
Shear flow versus mechanical compression	MTHFD1	Methylenetetrahydrofolate dehydrogenase 1	Synergistic effect (short duration, high expression)
	GART	Phosphoribosylglycinamide formyltransferase	Synergistic effect (short duration, high expression)
Tensile stretch versus mechanical compression	UHRF1	Ubiquitin like with PHD and ring finger domains 1	Synergistic effect (short duration, high expression)
	RPL35A	Ribosomal protein L35a	N/C (high expression under 0.1-Hz stretch and short-duration compression)
	HIST1H1B	Histone cluster 1 H1 family member b	N/C (high expression under 0.1-Hz stretch and high-amplitude compression)

[a]Cooperative action under comparable loading parameters between the two distinct stimuli

[b]Not correlated (N/C) between the two distinct stimuli without comparable loading parameter

## 3.5 Constructing the co-expressed network under combined mechanical stimuli

To further elucidate the potential mechanisms of molecular interactions among three stimuli, a WGCNA analysis was applied to construct the co-expression network and present the functional modules (Langfelder and Horvath 2008). Hierarchical clustering of all the genes screened under three stimuli constructed the cluster dendragram, in which six modules were classified to define the correlation and clustering among these modules (Fig. 6a). Heatmap of co-expression network or eigengene adjacency represented the degree of gene correlation, in which the darker the color is the higher the correlation yields between any two genes in the entire gene set (Fig. 6b). The same colored genes yielded high correlation and clustering among six modules (Fig. 6c).

Correlation coefficients and *p*-values between the modules (*y*-axis) and the mechanical parameters (*x*-axis) are summarized in Fig. 6d. Here red and blue boxes denoted the positive and negative correlations, respectively, in a darkness-dependent manner. Picking up *green* and *blue* modules as an example to test their correlation differences in compression amplitude, the *green* module was positively correlated with 200 kPa but negatively with 20 kPa, whereas *blue* module was reversed. GO analysis was then conducted and the outcomes were compared with those obtained from GSEA analysis. For *green* module genes, the enriched terms were similar to those in high compression amplitude from

GSEA analysis (Fig. S5b–d), such as mitochondria-related sets in CC (Fig. S6a), cell respiration-related sets in BP (Fig. S6b), and oxidative phosphorylation-related sets in MF (Fig. S6c). By contrast, *blue* module genes enrichment defined ficolin-1-related protein and myelin sheath component in CC, which are in coincidence with GSEA analysis (Figs. S6d; cf. S5b). Those enriched in BP (Fig. S6e) and MF (Fig. S6f) are not identical to those from GSEA analysis (cf. Fig. S5c–d). Collectively, *green* module genes enrichment is in excellent agreement with GSEA in CC, BP, and MF, but *blue* module genes enrichment is similar only in CC. Considering their methodological differences, the outcomes from these analyses are comparable and reliable.

3.6 Effects of mechanical stimulation on nucleolus phenotype

There is a possibility that the phenotype or function of hESC was changed after application of mechanical stimuli. Considering that nucleolar size and RNA content are well-defined indicators for protein synthesis and cell proliferation (Derenzini et al. 2000), the nuclear features, especially for nucleolus, were characterized by immunostaining before and after typical stretch, flow and compression. Under intermittent stretch at 0.1 Hz for 12 h, the nucleolus became clear with confined contour and its area was increased significantly (Fig. 7a–c). rRNA expression was also enhanced in the nucleolus with higher mean (MFI) or total fluorescence
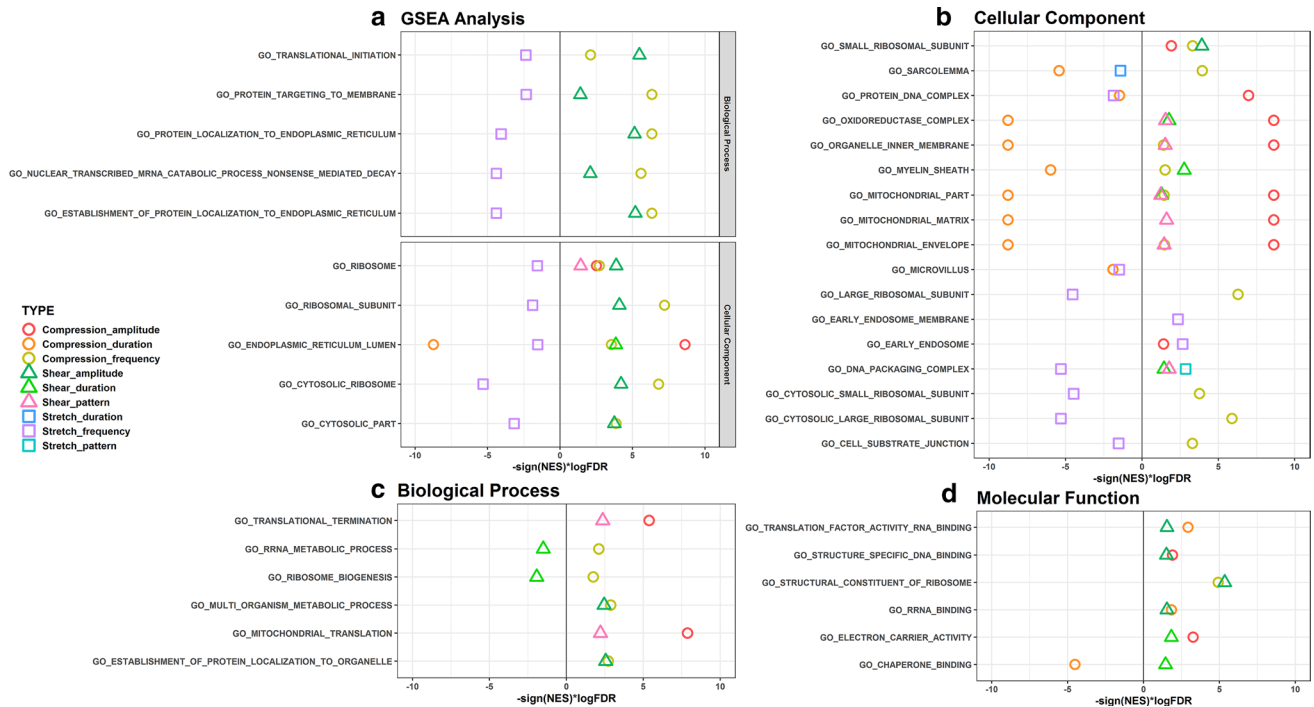
Fig. 5 Enrichment analysis of GSEA commonly shared under distinct mechanical stimuli. Plotted were the commonly shared, enriched terms for cellular component (CC) and biological process (BP) sets under all the three stimuli **a**, as well as for CC **b**, BP **c**, and molecular function (MF) **d** sets between any two of three stimuli. The terms were enriched by setting FDR < 25% as the threshold after GSEA-P analysis. Squares, triangles, and circles denote the various cases of tensile stretch, shear flow, and mechanical compression, respectively. Here the absolute value of *x*-axis is defined as logFDR, and the larger value depicts the higher reliability of enrichment results. Sign (NES) in *x*-axis defines the direction of enrichment upon the following definitions of FC values: For tensile stretch, pattern ~ I/C, frequency ~ 1-Hz/0.1-Hz, and duration ~ 1-h/12-h; for shear flow, pattern ~ S/P, amplitude ~ 1.1-Pa/0.5-Pa, and duration ~ 1-h/24-h; for mechanical compression, amplitude ~ H/L, frequency ~ 1-Hz/0.1-Hz, and duration ~ 1-h/12-h (also refer to Fig S5a). Here the positive and negative values represent the enrichment towards the directions represented by numerator and denominator, respectively

intensity (TFI) than those in static controls (Fig. 7d–e), consistent with the relevant GSEA enrichment analyses in ribosome- and translation-related terms (Figs. 7f and S7a–c). The same pattern was also observed under steady shear flow at 1.1 Pa for 24 h. Here the nucleolus became significantly larger with stronger rRNA staining than those in static controls and the ribosome- and translation-related terms were evidently enriched (Figs. 7g–l and S7d–f). By contrast, slightly different patterns were found under cyclic compression of 20 kPa at 1 Hz for 1 h. While no difference in the nucleolus area was observed between compression and static control (Fig. 7m–o), the increase of nucleolar RNA staining was still noticeable (Fig. 7p–q), consistent with the enrichment of ribosome- and translation-related terms (Figs. 7r and S7g–l) as those under stretch or shear. These results suggested that more rRNAs could be synthesized under different mechanical stimuli.

We also examined the effect of mechanical stimuli on nucleus morphology and DNA expression (Fig. S8). No significant differences were visualized on nuclear area, circularity, aspect ratio, and DNA expression under stretch compared to static control (Fig. S8a–e). Similar patterns were observed under shear with constant nuclear circularity, aspect ratio, and total DNA expression (Fig. S8g, h, j), even though the area was enlarged (Fig. S8f) and mean DNA expression was reduced (Fig. S8i). Again, no difference were found under compression for nucleus area and mean or total DNA expression (Fig. S8k, n, o) whereas nucleus circularity was relative increased (Fig. S8l) and the aspect ratio was slightly reduced (Fig. S8m). Collectively, various mechanical stimuli tended to enhance nucleolus area and rRNA expression while nucleus morphology and DNA expression remained unchanged (Figs. 7 and S8).

4 Discussions

Nowadays, comprehensive understanding is obtained to elucidate the mechanical responses of cells in vivo, since cells usually reside in a complex and diverse microenvironment where multiple types of mechanical stimuli are present. Each type of the stimuli contains several loading parameters such as pattern, amplitude, frequency, and duration. Thus the relevant observations in biological functions are usually
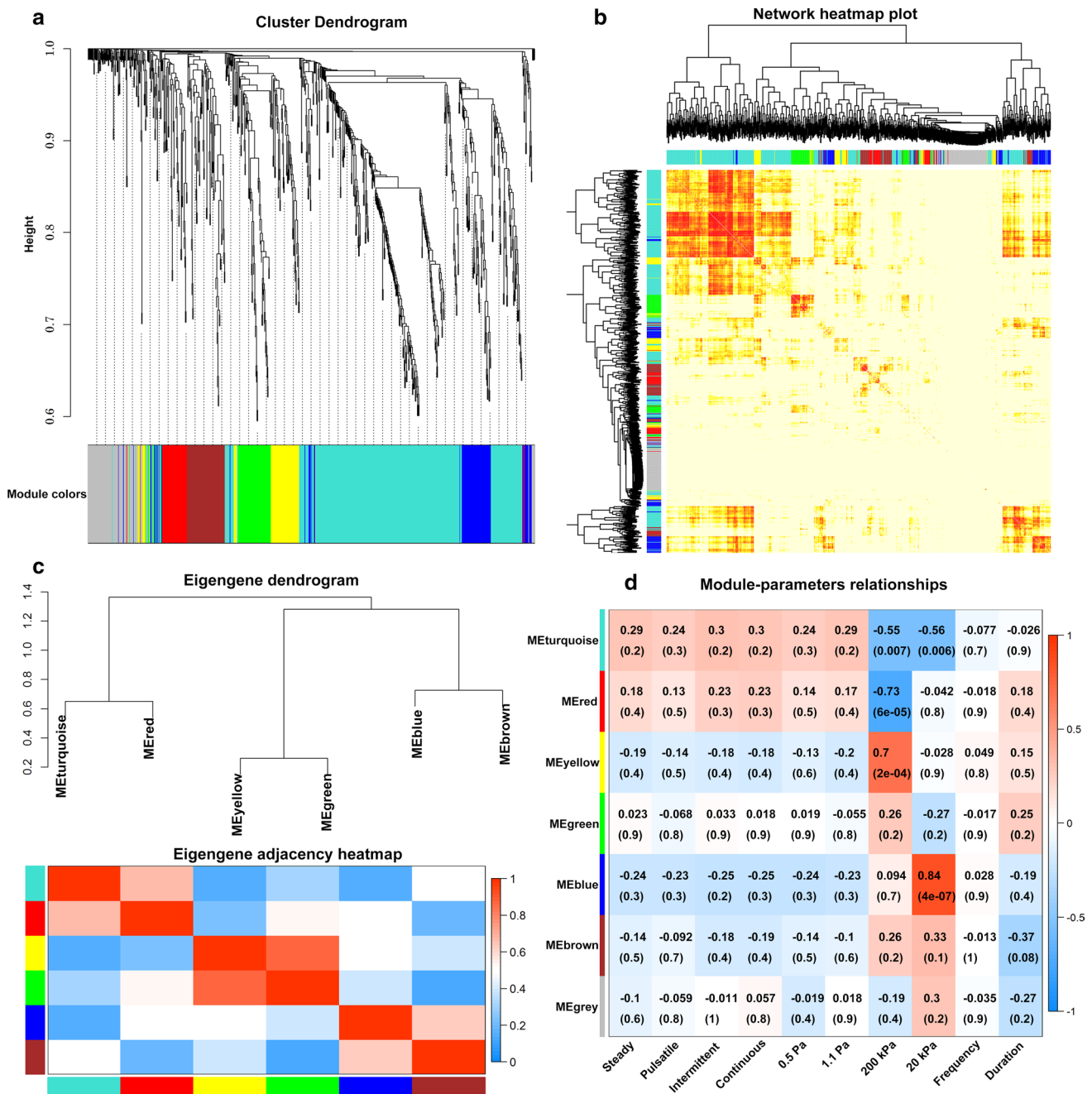
Fig. 6 WGCNA analysis of co-expression network under distinct mechanical stimuli. **a** Cluster dendrogram of commonly-shared proteins under all the three stimuli, which is segregated into six expression modules. **b** Co-expression network heatmap. The darker the color is the higher correlation yields. **c** Eigengene dendrogram and eigengene adjacency heatmap of six expression modules. **d** Correlation coefficients and p-values between expression modules and loading parameters. Red and blue boxes inside each module define the positive and negative correlations, respectively, and the darker the color is the higher correlation yields. The grey row at the bottom denoted those protein that cannot be included in the above six modules

parameter-dependent (Wang et al. 2014). Here we adopted the global factorial settings by mimicking physiologically like mechanical combinations for hESCs and characterized their proteomic profiling, making the screened proteins more reasonable and universal. The relevant bioinformatics analyses implied a universal mechanism under tensile stretch,

shear flow, and mechanical compression from the viewpoint of "mechanomics" (van Loon 2009; Wang et al. 2014). The novel findings lie in at least three aspects. First, mechanosensitive proteins were highly correlated with the combination of pattern, amplitude, frequency, and duration from a single type of mechanical stimulus used. Second, only a few
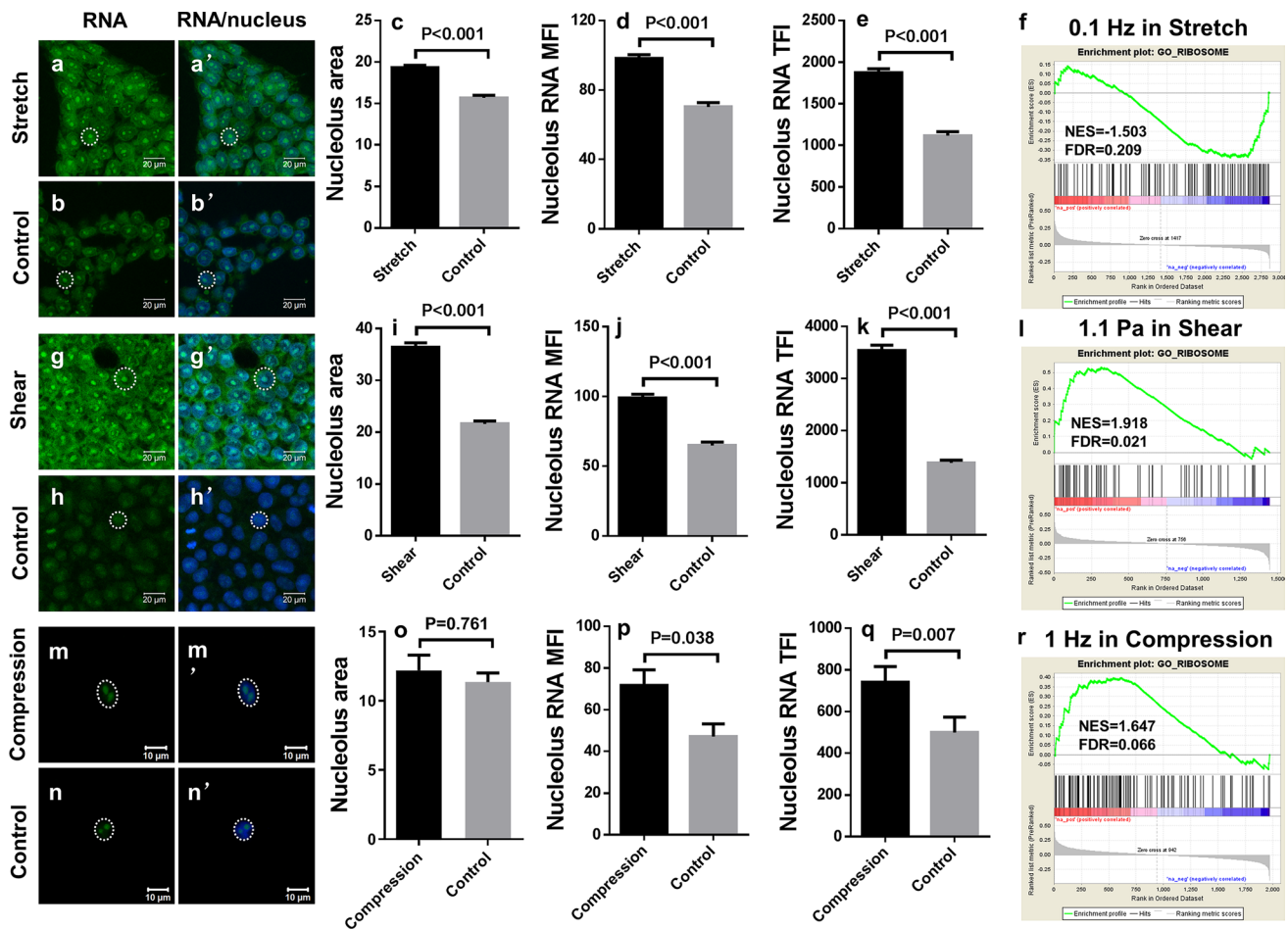
Fig. 7 Validation of rRNA expression and the related GSEA analysis under typical stretch **a–f**, shear **g–i** and compression **m–r**. Nucleolus rRNA staining was presented under stretch **a**, shear **g** and compression **m** and the respective controls **b**, **h**, **n** and also merged with Hoechst 33,342 staining for nuclei under stretch **a'**, shear **g'** and compression **m'** and the controls **b'**, **h'**, **n'**. Nucleolus area and mean or total fluorescence intensity (MFI or TFI) of rRNA under stretch **c–e**, shear **i–k** and compression **o–q** were obtained from three or four inde-pendent repeats and presented as the mean ± SE. Total cell number measured was 150 and for stretch, 100–110 for shear, and 47–53 for compression. Also illustrated was the ribosome enrichment at 0.1 Hz under stretch **f**, 1.1 Pa under shear **i** and 1 Hz under compression **r** from GSEA analysis. Dotted cycles in the left two columns indicated those typical nucleoli, respectively. Scale bar = 20 μm in **a**, **b**, **g**, **h** and scale bar = 10 μm in **m**, **n**

mechanosensitive proteins were identified from two or three types of mechanical stimuli combined. Third, common bio-logical functions in protein synthesis and modification were found among three mechanical stimuli while other functions specific in skin development were correlated to individual mechanical stimuli. This work is the first mechanomics study on hESCs, highlighting the potential roles of those key pro-teins in mechanical responses of cells.

Unlike those works under single mechanical stimulus, mechanomics analysis implied that the mechanosensing mechanisms of hESCs are complicated in response to the combined stimulating types and loading parameters. In this work, only two core hub proteins, GART and EXOSC5, were co-expressed across two types of mechanical stimuli (Fig. 4). The former is found between shear and compression and

associated with a key catalytic action in ab initio synthesis of purines (Warren and Buchanan 1957). The latter, which has 3′→5′ exoribonuclease activity and is related to RNA maturation and degradation, is presented between shear and compression (Chen et al. 2001; Mukherjee et al. 2002). Functions of the two mechanosensitive molecules are related to energy metabolism, biosynthesis, and transcriptional regulation, and GART also serves as a target candidate for antitumor drug design from the viewpoint of mechanomedi-cine (Costi and Ferrari 2001). Although the two proteins were not reported for other cell types, these hub proteins are likely cell type-specific under different mechanical stimuli. In addition to these core hub proteins, other mechanosensi-tive proteins are also crucial for future mechanobiological studies (Tables 1 and S4). To emphasize their importance,

the differentially expressed proteins were compared even though the direct comparisons with the data of hESCs are not available (Fig. 8). For example, stretching astrocytes at 12% and 1 Hz significantly up-regulates ANXA4 expression (Rogers et al. 2012), positively correlating to a 1.1-fold enhancement from continuous to intermittent stretch (Fig. 8a). Under steady laminar flow of 1–2 Pa, β1-integrin expression in bovine aortic endothelial cells is transiently increased up to the peak at 1 h and then decayed gradually (Li et al. 2005), consistent with current data that 1-h expression is 1.15-fold higher than 24-h expression (Fig. 8b). Static compression on chondrocytes at 30 MPa for 6 h results in dramatic increase of HSP70 expression (Li et al. 2011), in agreement with a 1.3-fold enhancement in HSPA2 (one member in HSP70 family) from 1-h to 12-h loading, and 1.23- and 1.28-fold enhancement in respective HSPA1A and HSPA4 (two members in HSP70 family) from 20- to 200-kPa loading (Fig. 8c). While these comparisons supported our mechanomics analyses typically case-by-case, they also indicated that mechanomics-based screening of mechano-sensitive molecules helps to identify the target molecules under physiologically-like mechanical environment.

The universal mechanotransductive mechanisms under distinct stimuli proposed here have potential significances in regulating the stemness and differentiation of embryonic stem cells. In mechanically induced mESC differentiation (Dado et al. 2012), those related findings seem to be quite complicated. For example, stretch could induce mESC (Dado-Rosenfeld et al. 2015) or derived EBs (Du

et al. 2017) into mesoderm while long- or short- stretch duration results in respective upregulation and downregulation of stemness marker NANOG in mESCs (Horiuchi et al. 2012) and hESCs (Saha et al. 2008). Shear stress also has similar outcomes. Stirring shear and laminar flow can promote the differentiation of hESCs ES03 (HES-3) (Leung et al. 2011) or mESCs (Illi et al. 2005; Nsiah et al. 2014; Sargent et al. 2010; Wolfe and Ahsan 2013). Oppositely, shear stress is somewhat favorable for pluripotency maintenance of mESCs after the withdrawal of LIF (Cormier et al. 2006; Fernandes et al. 2007; Fok and Zandstra 2005; Shafa et al. 2011). In addition to these type- or pattern-dependent biological variations, the complicated mechanical parameter sets are also responsible for these controversies. For example, tensile frequency is a key parameter to induce the diverse differentiation of hESC-derived cardiomyocyte (hESC-CM), where applying 1 and 3 Hz results in a significant decrease and increase, respectively, in cardiogenic gene expression (Shimko and Claycomb 2008). mESCs also respond to flow parameters in different ways, that is, the exposure to high and low shear stress results in the increased ectodermal genes and the decreased mesodermal genes, respectively, and loading in long shear duration promotes mesodermal genes (T-BRACHY) and suppresses endoderm genes (AFP), but, in short duration, promotes ectodermal genes (Wolfe et al. 2012). Therefore, the type, pattern, and parameter set are all crucial when elucidating the impacts of specific mechanical stimuli on ESCs. Mechanomics analysis is able to evaluate the potential biological functions under
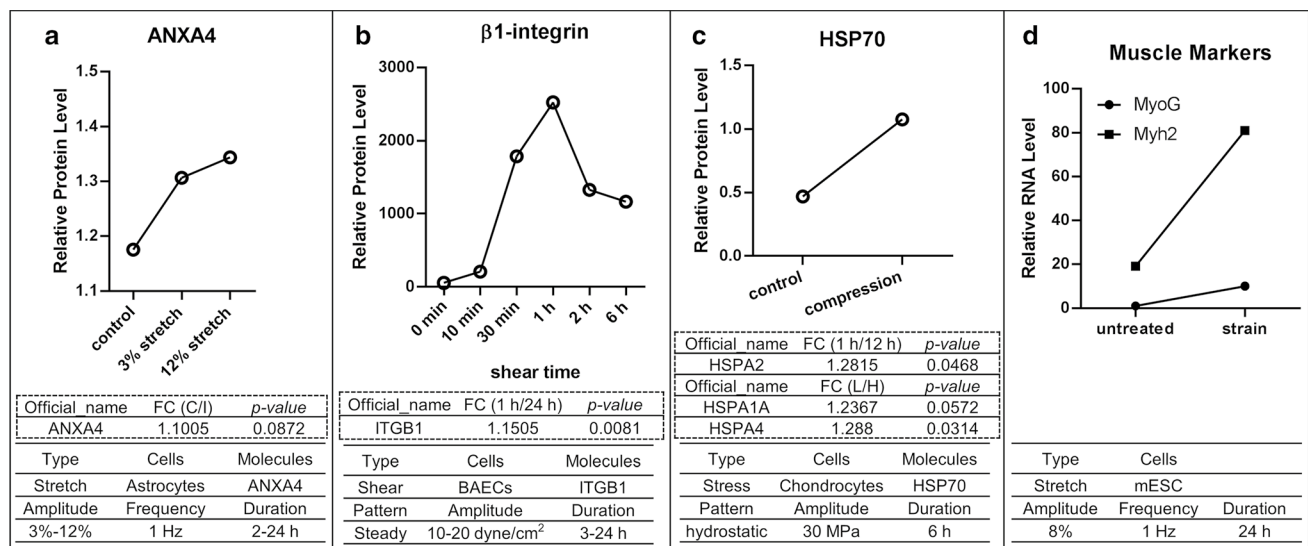
Fig. 8 Typical comparisons of mechanosensitive proteins between current mechanomics analysis and those mechanobiological measurements in the literatures. **a–c** Mechanosensitive proteins screened in tensile stretch (**a**; Rogers et al. 2012), shear flow (**b**; Li et al. 2005), and mechanical compression (**c**; Li et al. 2011), respectively, were adopted from the literatures and re-plotted as the upper curves together with the lower tables. The dotted box between the curve and the table in each panel denotes the typical protein screened from the current mechanomics analysis. **d** Comparison of GSEA functional enrichment analysis from the current work with those typical functional tests in the literatures (Tannaz et al. 2014)

combined types or parameters of mechanical stimuli. As an example, mESCs exposed to a mechanical strain of 1 Hz, 8% elongation for 24 h could be differentiated into skeletal muscle lineage (Fig. 8d) (Tannaz et al. 2014). Meanwhile, a tensile stretch for 12 h potentiated hESCs differentiating into muscle cells (as seen in enriched "sarcolemma" terms in long stretch duration in Fig. 5b), while none of similar enrichment terms was observed upon stretch pattern and frequency (Figs. 5a and S5). Thus, the different mechanical cues responsible for the special biological processes can be isolated readily (Figs. 5 and S5).

The link among stretch, shear and compression is highly complicated, yielding both similarities and differences when cells perceive different mechanical stimuli. On the one hand, differentially expressed proteins derived from distinct stimuli were overlapped with each other and consistent regulations of these proteins were also observed on specialized loading parameters from varied stimuli (Table 1), as seen in those similar biological functions enriched by GSEA analyses. H1 cells were consistently responsive to 12-h loading duration between stretch and compression with an enriched "sarcolemma" term (Fig. 5b), suggesting that the expression of shared proteins and related biological functions may be mutually reinforced under the two stimuli. On the other hand, protein synthesis was regulated reversely by loading frequency between stretch and compression. Typical terms of "oxidoreductase complex," "mitochondrial part" and "myelin sheath" were enriched differently under short-duration (1-h) shear and long-duration (24-h) compression (Fig. 5b), implying that those biological functions may conversely response to varied loading types and parameters. Indeed, shear flow does not affect hESC pluripotency, cell cycle and cell apoptosis but consolidate the primed state by enhancing rRNA synthesis in nucleolus (Wang et al. 2019) for function performance and pluripotency maintenance (Eleuteri et al. 2018; Percharde et al. 2018). Our results here also indicated that three mechanical stimuli significantly increased the expression of rRNA in nucleolus (Fig. 7), suggesting that mechanical stimulus could initiate phenotypic variations of the cells even with longer or stronger loading. Although different types of mechanical stimuli applied synchronously is not studied in this work, the above analyses infer that there are mutually agonistic or antagonistic responses among tensile stretch, shear flow, and mechanical compression, similar to positive and negative feedbacks of mechanical regulations in morphogenesis (Gilmour et al. 2017).

Technically, partial differences of functional enrichment in CC, BP, and MF were also observed between WGCNA and GSEA analyses (Figs. 6 and S6), which lies in two aspects. First, different gene sets were used to construct the co-expression networks from the two methods, *that is*, only the mechanically shared sets for the former and the entire sets in each case for the latter. Second, different rationales on screening co-expressed proteins were applied, where the former utilizes the expression-ranked modules for GO enrichment and the latter takes the advantages of the total expression matrix to screen the enriched terms. Meanwhile, loading parameters were systematically varied in a single type of mechanical stimuli but the cross-talk effect of distinct types of the stimuli is still not fully defined due to the technical difficulties of simultaneous loading of all three mechanical stimuli, which is more important in vivo. Moreover, a few mechanosensitive molecules, such as RhoA (Reffay et al. 2014), MAPK, and YAP (Liu et al. 2016), are potentially activated by phosphorylation, which are difficult to uncover from conventional proteomics analysis. Thus, phosphorylation proteomics analysis is also required to elaborate those precise changes in the future.

Authors' contributions ML, JW, FZ and DL conceived the project; FZ, JW and DL performed the experiments and analyzed the data; DL and LZ prepared the hESCs and analyzed the data; BS compiled the pump control software; YG designed the flow chamber; YW analyzed the data and prepared the figures; ML, ZF, JW, and DL wrote the paper.

Compliance with ethical standards

Conflict of interest The authors declare no competing financial interests.

References

Adamo L, Naveiras O, Wenzel PL, McKinney-Freeman S, Mack PJ, Gracia-Sancho J, Suchy-Dicey A, Yoshimoto M, Lensch MW, Yoder MC, García-Cardeña G, Daley GQ (2009) Biomechanical forces promote embryonic haematopoiesis. Nature 459:1131–1135. https://doi.org/10.1038/nature08073

Behrndt M, Salbreux G, Campinho P, Hauschild R, Oswald F, Roensch J, Grill SW, Heisenberg CP (2012) Forces driving epithelial spreading in zebrafish gastrulation. Science 338:257–260. https://doi.org/10.1126/science.1224143

Bindea G, Mlecnik B, Hackl H, Charoentong P, Tosolini M, Kirilovsky A, Fridman WH, Pagès F, Trajanoski Z, Galon J (2009) ClueGO: a Cytoscape plug-in to decipher functionally grouped gene ontology and pathway annotation networks. Bioinformatics 25:1091–1093. https://doi.org/10.1093/bioinformatics/btp101

Bonassar LJ, Grodzinsky AJ, Frank EH, Davila SG, Bhaktav NR, Trippel SB (2001) The effect of dynamic compression on the response of articular cartilage to insulin-like growth factor-I. J Orthop Res 19:11–17. https://doi.org/10.1016/s0736-0266(00)00004-8

Braet F, Shleper M, Paizi M, Brodsky S, Kopeiko N, Resnick N, Spira G (2004) Liver sinusoidal endothelial cell modulation upon

resection and shear stress in vitro. Comp Hepatol 3:7–7. https://doi.org/10.1186/1476-5926-3-7

Chahine MN, Dibrov E, Blackwood DP, Pierce GN (2012) Oxidized LDL enhances stretch-induced smooth muscle cell proliferation through alterations in nuclear protein import. Can J Physiol Pharmacol 90:1559–1568. https://doi.org/10.1139/y2012-141

Chen CY, Gherzi R, Ong SE, Chan EL, Raijmakers R, Pruijn GJ, Stoecklin G, Moroni C, Mann M, Karin M (2001) AU binding proteins recruit the exosome to degrade ARE-containing mRNAs. Cell 107:451–464. https://doi.org/10.1016/s0092-8674(01)00578-5

Chin CH, Chen S-H, Wu HH, Ho CW, Ko MT, Lin CY (2014) cytoHubba: identifying hub objects and sub-networks from complex interactome. BMC Syst Biol 8:S11. https://doi.org/10.1186/1752-0509-8-s4-s11

Chu TJ, Peters DG (2008) Serial analysis of the vascular endothelial transcriptome under static and shear stress conditions. Physiol Genomics 34:185–192. https://doi.org/10.1152/physiolgenomics.90201.2008

Cole RJ (1967) Cinemicrographic observations on the trophoblast and zona pellucida of the mouse blastocyst. J Embryol Exp Morphol 17:481–490

Conway A, Schaffer DV (2012) Biophysical regulation of stem cell behavior within the niche. Stem Cell Res Ther 3:50. https://doi.org/10.1186/scrt141

Cormier JT, Nieden NIZ, Rancourt DE, Kallos MS (2006) Expansion of undifferentiated murine embryonic stem cells as aggregates in suspension culture Bioreactors. Tissue Eng 12:3233–3245. https://doi.org/10.1089/ten.2006.12.3233

Costi M, Ferrari S (2001) Update on antifolate drugs targets. Curr Drug Targets 2:135–166. https://doi.org/10.2174/1389450013348669

Dado-Rosenfeld D, Tzchori I, Fine A, Chen-Konak L, Levenberg S (2015) Tensile forces applied on a cell-embedded three-dimensional scaffold can direct early differentiation of embryonic stem cells toward the mesoderm germ layer. Tissue Eng Part A 21:124–133. https://doi.org/10.1089/ten.tea.2014.0008

Dado D, Sagi M, Levenberg S, Zemel A (2012) Mechanical control of stem cell differentiation. Regen Med 7:101–116. https://doi.org/10.2217/rme.11.99

Derenzini M, Trere D, Pession A, Govoni M, Sirri V, Chieco P (2000) Nucleolar size indicates the rapidity of cell proliferation in cancer tissues. J Pathol 191:181–186. https://doi.org/10.1002/(SICI)1096-9896(200006)191:2<181:AID-PATH607>3.0.CO;2-V

Du V, Luciani N, Richard S, Mary G, Gay C, Mazuel F, Reffay M, Menasché P, Agbulut O, Wilhelm C (2017) A 3D magnetic tissue stretcher for remote mechanical control of embryonic stem cell differentiation. Nat Commun 8:400. https://doi.org/10.1038/s41467-017-00543-2

Eleuteri B, Aranda S, Ernfors P (2018) NoRC recruitment by H2A.X deposition at rRNA gene promoter limits embryonic stem cell proliferation. Cell Rep 23:1853–1866. https://doi.org/10.1016/j.celrep.2018.04.023

Elosegui-Artola A, Andreu I, Beedle AEM, Lezamiz A, Uroz M, Kosmalska AJ, Oria R, Kechagia JZ, Rico-Lastres P, Le Roux AL, Shanahan CM, Trepat XT, Navajas D, Garcia-Manyes S, Pere Roca-Cusachs P (2017) Force triggers YAP nuclear entry by regulating transport across nuclear pores. Cell 171:1397–1410. https://doi.org/10.1016/j.cell.2017.10.008

Fernandes AM, Fernandes TG, Diogo MM, da Silva CL, Henrique D, Cabral JMS (2007) Mouse embryonic stem cell expansion in a microcarrier-based stirred culture system. J Biotechnol 132:227–236. https://doi.org/10.1016/j.jbiotec.2007.05.031

Fok EYL, Zandstra PW (2005) Shear-controlled single-step mouse embryonic stem cell expansion and embryoid body-based differentiation. Stem Cells 23:1333–1342. https://doi.org/10.1634/stemcells.2005-0112

Gilmour D, Rembold M, Leptin M (2017) From morphogen to morphogenesis and back. Nature 541:311–320. https://doi.org/10.1038/nature21348

Heisenberg CP, Bellaiche Y (2013) Forces in tissue morphogenesis and patterning. Cell 153:948–962. https://doi.org/10.1016/j.cell.2013.05.008

Herranz R, Larkin OJ, Dijkstra CE, Hill RJA, Anthony P, Davey MR, Eaves L, van Loon JJWA, Medina FJ, Marco R (2012) Microgravity simulation by diamagnetic levitation: effects of a strong gradient magnetic field on the transcriptional profile of Drosophila melanogaster. BMC Genomics 13:52. https://doi.org/10.1186/1471-2164-13-52

Horiuchi R, Akimoto T, Hong Z, Ushida T (2012) Cyclic mechanical strain maintains Nanog expression through PI3K/Akt signaling in mouse embryonic stem cells. Exp Cell Res 318:1726–1732. https://doi.org/10.1016/j.yexcr.2012.05.021

Horner VL, Wolfner MF (2008) Mechanical stimulation by osmotic and hydrostatic pressure activates Drosophila oocytes in vitro in a calcium-dependent manner. Dev Biol 316:100–109. https://doi.org/10.1016/j.ydbio.2008.01.014

Huang HY, Nakayama Y, Qin K, Yamamoto K, Ando J, Yamashita J, Itoh H, Kanda K, Yaku H, Okamoto Y, Nemoto Y (2005) Differentiation from embryonic stem cells to vascular wall cells under in vitro pulsatile flow loading. J Artif Organs 8:110–118. https://doi.org/10.1007/s10047-005-0291-2

Hur YS, Park JH, Ryu EK, Yoon HJ, Yoon SH, Hur CY, Lee WD, Lim JH (2011) Effect of artificial shrinkage on clinical outcome in fresh blastocyst transfer cycles. Clin Exp Reprod Med 38:87–92. https://doi.org/10.5653/cerm.2011.38.2.87

Illi B, Scopece A, Nanni S, Farsetti A, Morgante L, Biglioli P, Capogrossi MC, Gaetano C (2005) Epigenetic histone modification and cardiovascular lineage programming in mouse embryonic stem cells exposed to laminar shear stress. Circ Res 96:501–508. https://doi.org/10.1161/01.RES.0000159181.06379.63

Ingber DE (2006) Cellular mechanotransduction: putting all the pieces together again. FASEB J 20:811–827. https://doi.org/10.1096/fj.05-5424rev

Ji JY, Jing H, Diamond SL (2003) Shear stress causes nuclear localization of endothelial glucocorticoid receptor and expression from the GRE promoter. Circ Res 92:279–285. https://doi.org/10.1161/01.res.0000057753.57106.0b

Jiang YK, Liu HW, Li H, Wang FJ, Cheng K, Zhou GD, Zhang WJ, Ye ML, Cao YL, Liu W, Zou HF (2011) A proteomic analysis of engineered tendon formation under dynamic mechanical loading in vitro. Biomaterials 32:4085–4095. https://doi.org/10.1016/j.biomaterials.2011.02.033

Krzywinski M, Schein J, Birol I, Connors J, Gascoyne R, Horsman D, Jones SJ, Marra MA (2009) Circos: an information aesthetic for comparative genomics. Genome Res 19:1639–1645. https://doi.org/10.1101/gr.092759.109

Kurpinski K, Chu J, Wang D, Li S (2009) Proteomic profiling of mesenchymal stem cell responses to mechanical strain and TGF-beta1. Cell Mol Bioeng 2:606–614. https://doi.org/10.1007/s12195-009-0090-6

Lam AP, Dean DA (2008) Cyclic stretch-induced nuclear localization of transcription factors results in increased nuclear targeting of plasmids in alveolar epithelial cells. J Gene Med 10:668–678. https://doi.org/10.1002/jgm.1187

Langfelder P, Horvath S (2008) WGCNA: an R package for weighted correlation network analysis. BMC Bioinformatics 9:559. https://doi.org/10.1186/1471-2105-9-559

Leeb C, Jurga M, McGuckin C, Forraz N, Thallinger C, Moriggl R, Kenner L (2011) New perspectives in stem cell research: beyond

embryonic stem cells. Cell Prolif 44:9–14. https://doi.org/10.1111/j.1365-2184.2010.00725.x

Lemaitre C, Bickmore WA (2015) Chromatin at the nuclear periphery and the regulation of genome functions. Histochem Cell Biol 144:111–122. https://doi.org/10.1007/s00418-015-1346-y

Leung HW, Chen A, Choo ABH, Reuveny S, Oh SKW (2011) Agitation can induce differentiation of human pluripotent stem cells in microcarrier cultures. Tissue Eng Part C Methods 17:165–172. https://doi.org/10.1089/ten.tec.2010.0320

Li J, Zhang F, Chen JY (2011) An integrated proteomics analysis of bone tissues in response to mechanical stimulation. BMC Syst Biol 5(Suppl 3):S7. https://doi.org/10.1186/1752-0509-5-S3-S7

Li YSJ, Haga JH, Chien S (2005) Molecular basis of the effects of shear stress on vascular endothelial cells. J Biomech 38:1949–1971. https://doi.org/10.1016/j.biomech.2004.09.030

Liu Z, Wu HJ, Jiang KW, Wang YJ, Zhang WJ, Chu QQ, Li J, Huang HW, Cai T, Ji HB, Yang C, Tang N (2016) MAPK-mediated YAP activation controls mechanical-tension-induced pulmonary alveolar regeneration. Cell Rep 16:1810–1819. https://doi.org/10.1016/j.celrep.2016.07.020

Malone AMD, Batra NN, Shivaram G, Kwon RY, You L, Kim CH, Rodriguez J, Jair K, Jacobs CR (2007) The role of actin cytoskeleton in oscillatory fluid flow-induced signaling in MC3T3-E1 osteoblasts. Am J Physiol Cell Physiol 292:C1830–C1836. https://doi.org/10.1152/ajpcell.00352.2005

Mangala LS, Zhang Y, He Z, Emami K, Ramesh GT, Story M, Rohde LH, Wu H (2011) Effects of simulated microgravity on expression profile of microRNA in human lymphoblastoid cells. J Biol Chem 286:32483–32490. https://doi.org/10.1074/jbc.M111.267765

McKee C, Hong Y, Yao D, Chaudhry GR (2017) Compression induced chondrogenic differentiation of embryonic stem cells in three-dimensional polydimethylsiloxane scaffolds. Tissue Eng Part A 23:426–435. https://doi.org/10.1089/ten.tea.2016.0376

Mootha VK, Lindgren CM, Eriksson KF, Subramanian AS, Sihag S, Lehar J, Puigserver P, Carlsson E, Ridderstråle M, Laurila E, Houstis N, Daly MJ, Patterson N, Mesirov JP, Golub TR, Tamayo P, Spiegelman B, Lander ES, Hirschhorn JN, Altshuler D, Groop LC (2003) PGC-1alpha-responsive genes involved in oxidative phosphorylation are coordinately downregulated in human diabetes. Nat Genet 34:267–273. https://doi.org/10.1038/ng1180

Motosugi N, Bauer T, Polanski Z, Solter D, Hiiragi T (2005) Polarity of the mouse embryo is established at blastocyst and is not prepatterned. Genes Dev 19:1081–1092. https://doi.org/10.1101/gad.1304805

Mukherjee D, Gao M, O'Connor JP, Raijmakers R, Pruijn G, Lutz CS, Wilusz J (2002) The mammalian exosome mediates the efficient degradation of mRNAs that contain AU-rich elements. EMBO J 21:165–174. https://doi.org/10.1093/emboj/21.1.165

Nithiananthan S, Crawford A, Knock JC, Lambert DW, Whawell SA (2016) Physiological fluid flow moderates fibroblast responses to TGF-β1. J Cell Biochem 118:878–890. https://doi.org/10.1002/jcb.25767

Nsiah BA, Ahsan T, Griffiths S, Cooke M, Nerem RM, McDevitt TC (2014) Fluid shear stress pre-conditioning promotes endothelial morphogenesis of embryonic stem cells within embryoid bodies. Tissue Eng Part A 20:954–965. https://doi.org/10.1089/ten.tea.2013.0243

Patwari P, Lee RT (2008) Mechanical control of tissue morphogenesis. Circ Res 103:234–243. https://doi.org/10.1161/CIRCRESAHA.108.175331

Percharde M, Lin CJ, Yin Y, Guan J, Peixoto GA, Bulut-Karslioglu A, Biechele S, Huang B, Shen X, Ramalho-Santos M (2018) A LINE1-nucleolin partnership regulates early development and ESC identity. Cell 174:391–405. https://doi.org/10.1016/j.cell.2018.05.043

Qi YX, Jiang J, Jiang XH, Wang XD, Ji SY, Han Y, Long DK, Shen BR, Yan ZQ, Chien S, Jiang ZL (2011) PDGF-BB and TGF-beta1 on cross-talk between endothelial and smooth muscle cells in vascular remodeling induced by low shear stress. Proc Natl Acad Sci USA 108:1908–1913. https://doi.org/10.1073/pnas.1019219108

Quinn TM, Grodzinsky AJ, Hunziker EB, Sandy JD (1998) Effects of injurious compression on matrix turnover around individual cells in calf articular cartilage explants. J Orthop Res 16:490–499. https://doi.org/10.1002/jor.1100160415

Reffay M, Parrini MC, Cochet-Escartin O, Ladoux B, Buguin A, Coscoy S, Amblard F, Camonis J, Silberzan P (2014) Interplay of RhoA and mechanical forces in collective cell migration driven by leader cells. Nat Cell Biol 16:217–223. https://doi.org/10.1038/ncb2917

Rogers RS, Dharsee M, Ackloo S, Sivak JM, Flanagan JG (2012) Proteomics analyses of human optic nerve head astrocytes following biomechanical strain. Mol Cell Proteomics. https://doi.org/10.1074/mcp.m111.012302

Saha S, Ji L, de Pablo JJ, Palecek SP (2008) TGFβ/Activin/Nodal pathway in inhibition of human embryonic stem cell differentiation by mechanical strain. Biophys J 94:4123–4133. https://doi.org/10.1529/biophysj.107.119891

Sanders MC, Way M, Sakai J, Matsudaira P (1996) Characterization of the actin cross-linking properties of the scruin-calmodulin complex from the acrosomal process of Limulus sperm. J Biol Chem 271:2651–2657. https://doi.org/10.1074/jbc.271.5.2651

Sargent CY, Berguig GY, Kinney MA, Hiatt LA, Carpenedo RL, Berson RE, McDevitt TC (2010) Hydrodynamic modulation of embryonic stem cell differentiation by rotary orbital suspension culture. Biotechnol Bioeng 105:611–626. https://doi.org/10.1002/bit.22578

Shafa M, Sjonnesen K, Yamashita A, Liu S, Michalak M, Kallos MS, Rancourt DE (2011) Expansion and long-term maintenance of induced pluripotent stem cells in stirred suspension bioreactors. J Tissue Eng Regen Med 6:462–472. https://doi.org/10.1002/term.450

Shannon P, Markiel A, Ozier O, Baliga NS, Wang JT, Ramage D, Amin N, Schwikowski B, Ideker T (2003) Cytoscape: a software environment for integrated models of biomolecular interaction networks. Genome Res 13:2498–2504. https://doi.org/10.1101/gr.1239303

Shimko VF, Claycomb WC (2008) Effect of mechanical loading on three-dimensional cultures of embryonic stem cell-derived cardiomyocytes. Tissue Eng 14:49–58. https://doi.org/10.1089/ten.2007.0092

Shin JH, Tam BK, Brau RR, Lang MJ, Mahadevan L, Matsudaira P (2007) Force of an actin spring. Biophys J 92:3729–3733. https://doi.org/10.1529/biophysj.106.099994

Sorescu GP, Sykes M, Weiss D, Platt MO, Saha A, Hwang J, Boyd N, Boo YC, Vega JD, Taylor WR, Jo H (2003) Bone morphogenic protein 4 produced in endothelial cells by oscillatory shear stress stimulates an inflammatory response. J Biol Chem 278:31128–31135. https://doi.org/10.1074/jbc.m300703200

Stolberg S, McCloskey KE (2009) Can shear stress direct stem cell fate? Biotechnol Prog 25:10–19. https://doi.org/10.1002/btpr.124

Subramanian A, Tamayo P, Mootha VK, Mukherjee S, Ebert BL, Gillette MA, Paulovich A, Pomeroy SL, Golub TR, Lander ES, Mesirov JP (2005) Gene set enrichment analysis: a knowledge-based approach for interpreting genome-wide expression profiles. Proc Natl Acad Sci U S A 102:15545–15550. https://doi.org/10.1073/pnas.0506580102

Tannaz NA, Ali SM, Nooshin H, Nasser A, Reza M, Amir A, Maryam J (2014) Comparing the effect of uniaxial cyclic mechanical stimulation and chemical factors on myogenin and Myh2 expression in mouse embryonic and bone marrow derived mesenchymal stem cells. Mol Cell Biomech 11:19–37

Thomson JA, Itskovitz-Eldor J, Shapiro SS, Waknitz MA, Swiergiel JJ, Marshall VS, Jones JM (1998) Embryonic stem cell lines derived from human blastocysts. Science 282:1145–1147. https://doi.org/10.1126/science.282.5391.1145

Truong T, Shams H, Mofrad MRK (2015) Mechanisms of integrin and filamin binding and their interplay with talin during early focal adhesion formation. Integr Biol (Camb) 7:1285–1296. https://doi.org/10.1039/c5ib00133a

van Loon JJWA (2009) Mechanomics and physicomics in gravisensing Microgravity. Sci Technol 21:159–167

Vella D, Zoppis I, Mauri G, Mauri P, Di Silvestre D (2017) From protein-protein interactions to protein co-expression networks: a new perspective to evaluate large-scale proteomic data. EURASIP J Bioinform Syst Biol 2017:6. https://doi.org/10.1186/s13637-017-0059-z

Wang JW, Lü DY, Mao DB, Long M (2014) Mechanomics: an emerging field between biology and biomechanics. Protein Cell 5:518–531. https://doi.org/10.1007/s13238-014-0057-9

Wang JW, Wu Y, Zhang X, Zhang F, Lü DY, Shangguan B, Gao YX, Long M (2019) Flow-enhanced priming of hESCs through H2B acetylation and chromatin decondensation. Stem Cell Res Ther 10:349. https://doi.org/10.1186/s13287-019-1454-z

Ward DF Jr, Salasznyk RM, Klees RF, Backiel J, Agius P, Bennett K, Boskey A, Plopper GE (2007) Mechanical strain enhances extracellular matrix-induced gene focusing and promotes osteogenic differentiation of human mesenchymal stem cells through an extracellular-related kinase-dependent pathway. Stem Cells Dev 16:467–480. https://doi.org/10.1089/scd.2007.0034

Warren L, Buchanan JM (1957) Biosynthesis of the purines. XIX. 2-Amino-N-ribosylacetamide 5'-phosphate (glycinamide ribotide) transformylase. J Biol Chem 229:613–626

Wickham H (2016) ggplot2: elegant graphics for data analysis. Springer, New York

Wolfe RP, Ahsan T (2013) Shear stress during early embryonic stem cell differentiation promotes hematopoietic and endothelial phenotypes. Biotechnol Bioeng 110:1231–1242. https://doi.org/10.1002/bit.24782

Wolfe RP, Leleux J, Nerem RM, Ahsan T (2012) Effects of shear stress on germ lineage specification of embryonic stem cells. Integr Biol (Camb) 4:1263–1273. https://doi.org/10.1039/c2ib20040f

Xu J, Khor KA, Sui J, Zhang J, Tan TL, Chen WN (2008) Comparative proteomics profile of osteoblasts cultured on dissimilar hydroxyapatite biomaterials: an iTRAQ-coupled 2-D LC-MS/MS analysis. Proteomics 8:4249–4258. https://doi.org/10.1002/pmic.200800103

Yu G, Wang LG, Han Y, He QY (2012) clusterProfiler: an R package for comparing biological themes among gene clusters. OMICS 16:284–287. https://doi.org/10.1089/omi.2011.0118